Preparation of bare nZVI and Ni/Fe NPs

In brief, 40 mL of 0.74 M $NaBH_4$ (98%, Acros, Belgium) water solution was added dropwise into 500 mL of a 7:3 ethanol/water mixture solution that contained 18.23 mL 0.5 M $FeCl_3 \cdot 9H_2O$ for bare nZVI synthesis. A certain volume of 0.5 M $NiCl_2 \cdot 6H_2O$ was added into the $FeCl_3 \cdot 9H_2O$ ethanol/water solution for Ni/Fe NP synthesis. The volume of $NiCl_2$ was determined by the Ni additive loading, which ranged from 0.5 to 20 wt.% (Ni/Fe mass ratio) in this study. The mixture was continuously mixed for 30 min at the rate of 350 rpm. The collected particles were centrifuged and washed by deoxygenated ethanol for several cycles and then stored in deoxygenated ethanol for further use.

$$Fe^{3+} + 3BH_4^- + 3H_2O \rightarrow Fe + 3B(OH)_3 + 10.5H_2$$

$$Ni^{2+} + 2BH_4^- + 6H_2O \rightarrow Ni + 3B(OH)_3 + 7H_2$$

Solid Phase Analysis

The morphologies were characterized by SEM (Hitachi S-4800, Japan) with energy-dispersive (EDS) X-ray spectroscopy for element analysis. The core-shell structure was observed using high-resolution TEM (JEOL 2010F, Japan) with selected-area electron diffraction (SAED) operated at 200 kV. Brunauer-Emmett-Teller (BET) surface areas were measured by a surface-area and porosimetry analyzer (Micromeritics 2020HD, USA). The crystalline characteristics were tested by an XRD device (Bruker AXS D8, Germany), using Cu *K* radiation at 40 kV and a step size of 0.02° 2θ at 0.2 s/step. XPS spectra were used to determine the surface element composition of nZVI particles. Region scans of Fe 2p, O 1s, and Ni 2p were performed. Curving fitting of the Fe2p high-resolution XPS spectra was carried out using (Thermo Fisher Scientific, Inc., USA). The Fe and O region scan curves were fitted to quantify the surface element contents. The Fe $2p_{3/2}$ profile was fitted using photoelectron peaks at 706.9, 709.6, 710.8, and 712.3 eV, corresponding to metallic iron (Fe^0), ferrous iron [Fe(II)], ferric iron [Fe(III)], and Fe(III)-satellite peaks, respectively. The O 1s profile was fitted using photoelectron peaks at 529.9, 531.2, and 532.5 eV, corresponding to $\equiv O^-$, ≡OH, and $\equiv OH_2$. The Ni 2p profile was observed for Ni^0 (852.3 eV) and Ni^{2+} (855.8 eV) (36–40).

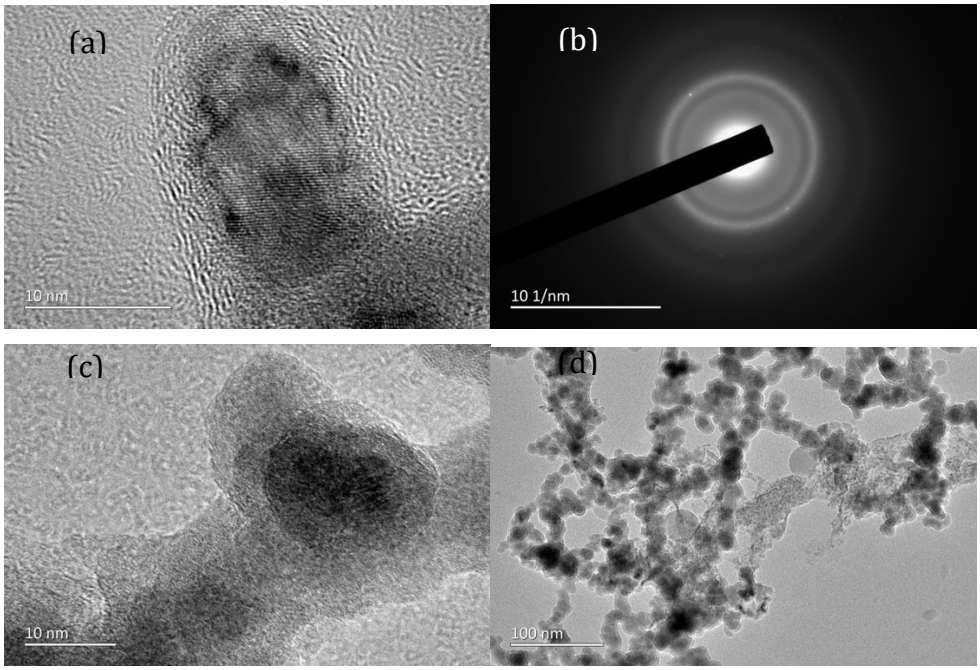

Fig. s1 HR-TEM of Ni/Fe 5wt%(a) and Ni/Fe 20wt%(c, d), SAED patter of Ni/Fe 5wt%(b)

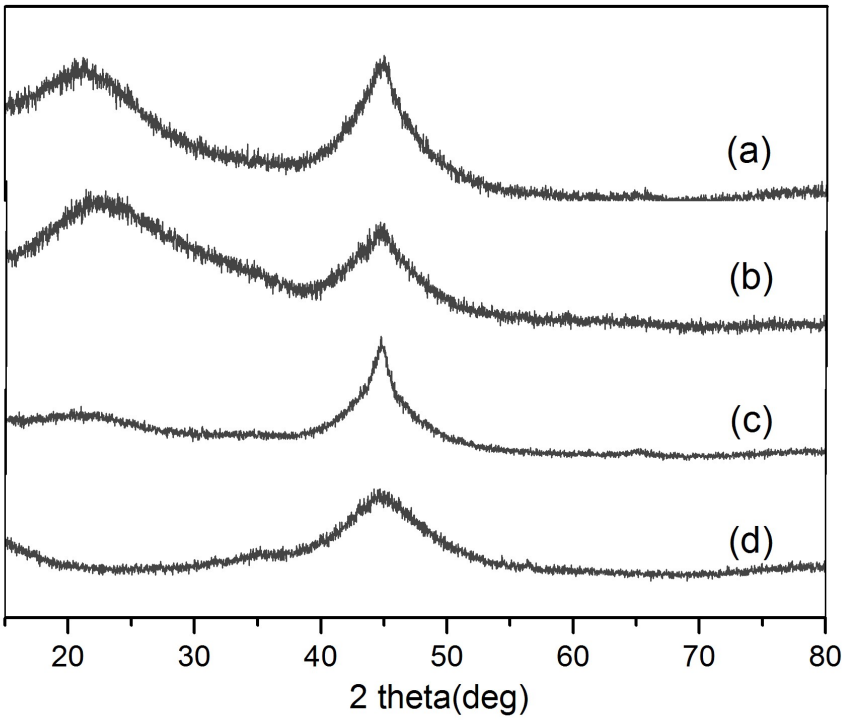

Figure s2 XRD patterns of as-synthesized Ni/Fe NPs: (a) Ni/Fe-0.5wt%, (b) Ni/Fe-3wt%, (c) Ni/Fe-5wt%, (d) Ni/Fe-20wt%.

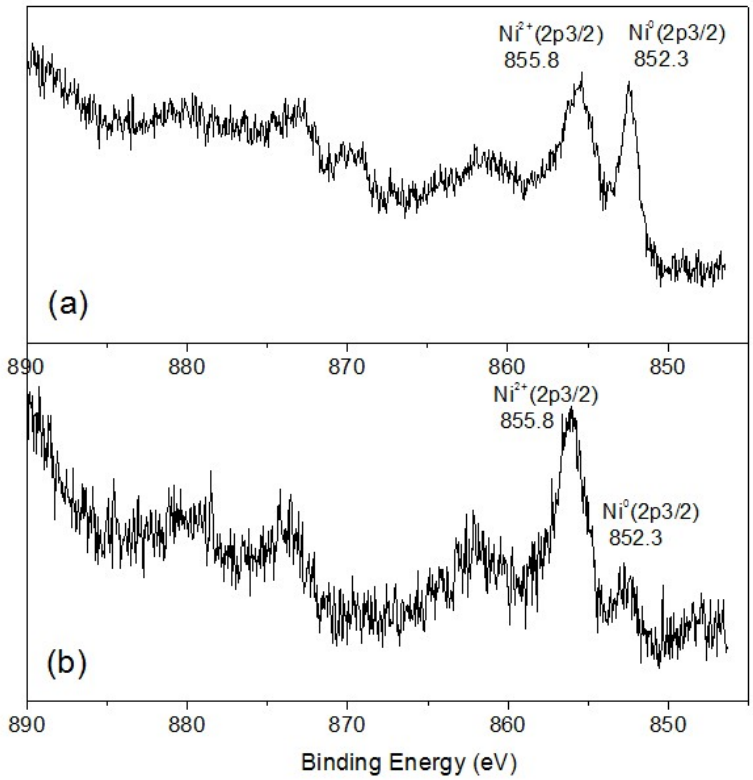

Figure s3 Ni2p XPS spectra of the 20wt% nickel added Ni/Fe NPs.

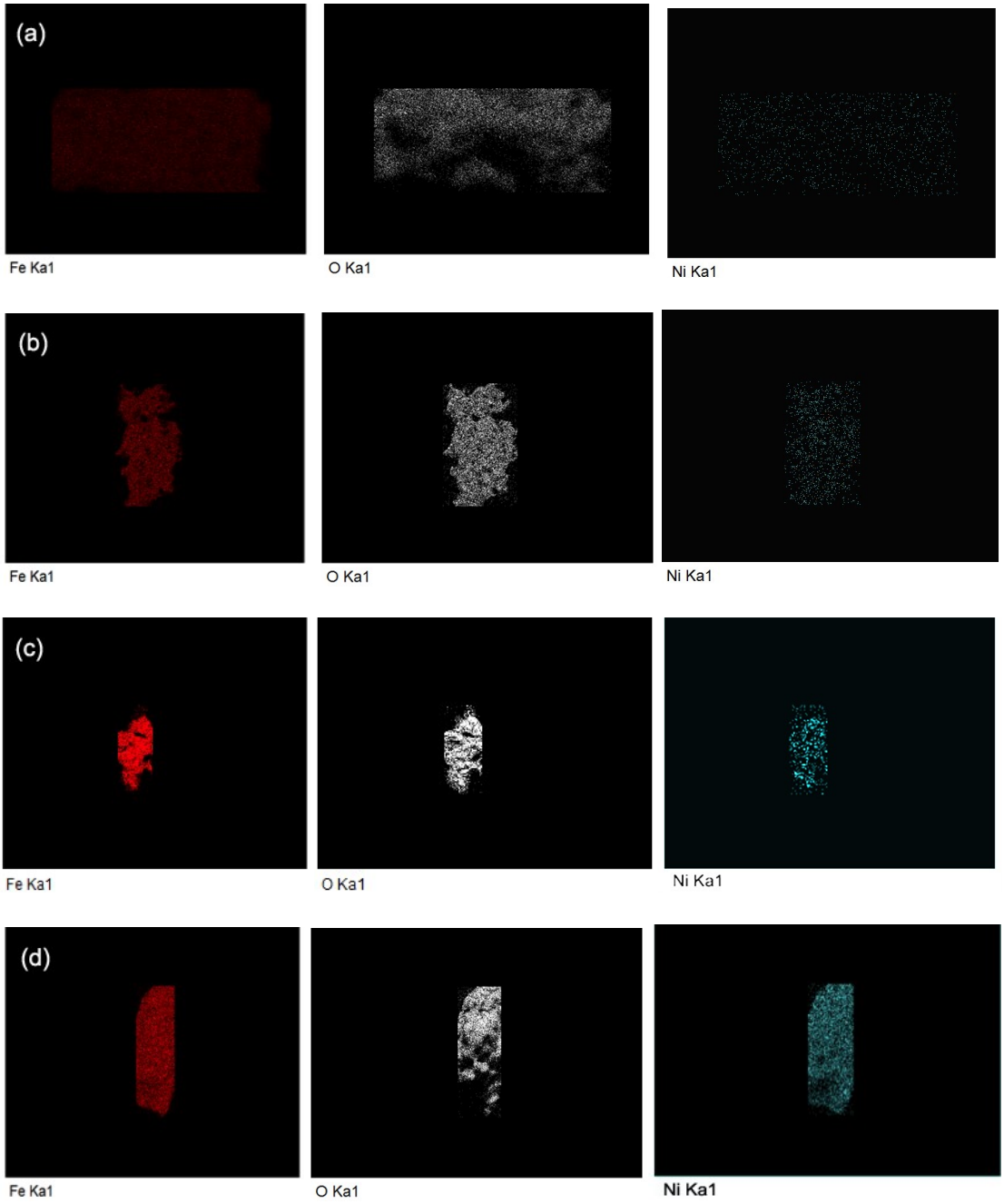

Figure s4 SEM-EDX mapping of bimetallic Ni/Fe NPs: (a) Ni/Fe-0.5wt%, (b) Ni/Fe-3wt%，(c) Ni/Fe-5wt%, and (d) Ni/Fe-20wt%.

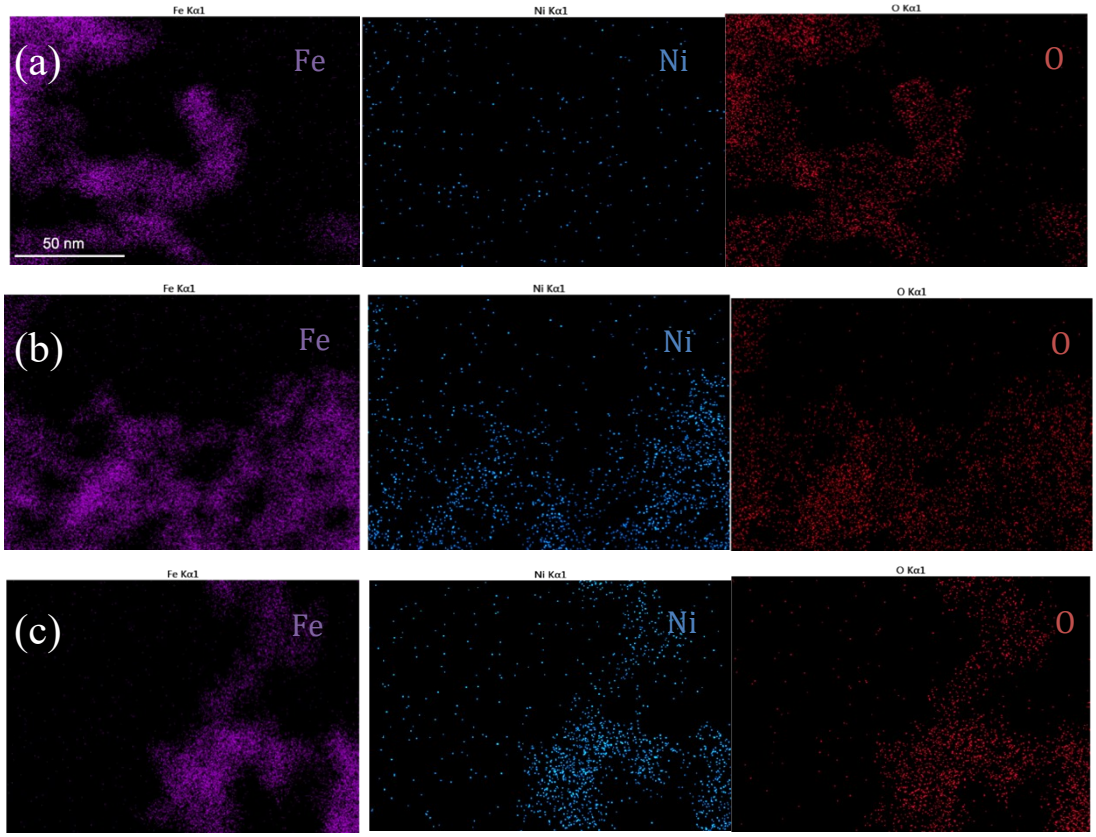

Figure s5 TEM-EDX mapping of Ni/Fe NPs: (a) Ni/Fe-0.5wt%, (b) Ni/Fe-5wt%, (c) Ni/Fe-20wt%.

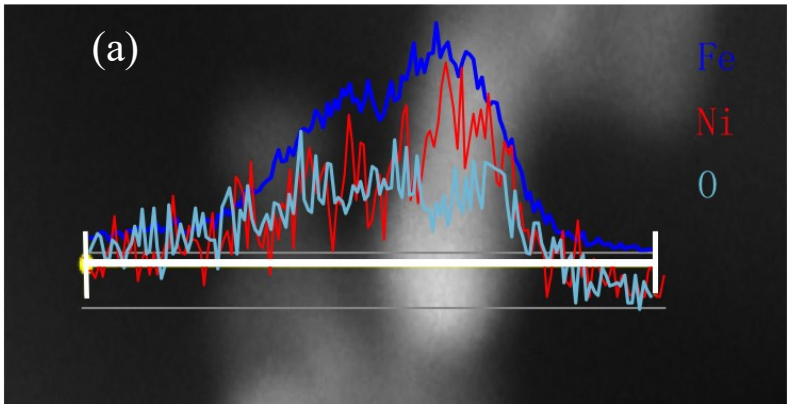

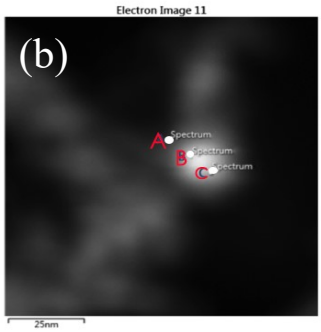

	Fe%	O%	Ni%
A	76.3	16.7	6.9
B	87.1	7.3	5.6
C	81.1	13.3	3.6

Figure s6 TEM-EDX line-scanning of the Ni/Fe-5wt%(a) and Ni/Fe-20wt%(b).

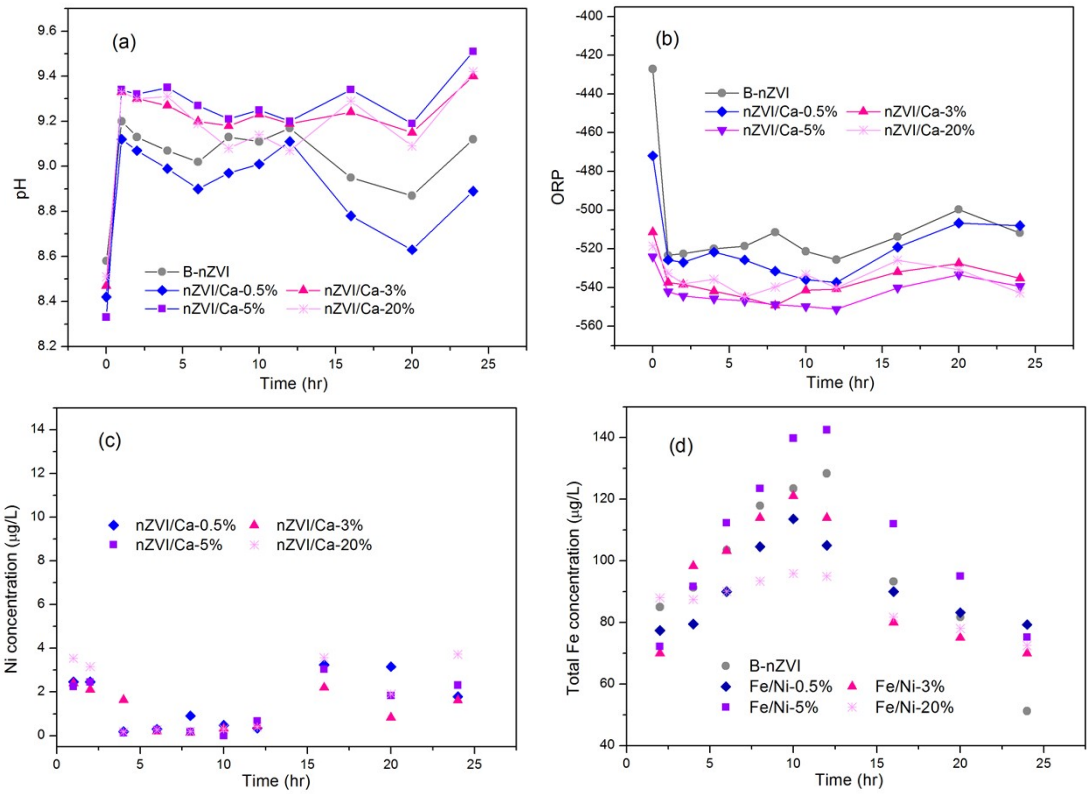

Figure s7 pH (a) and ORP change (b), Ni release (c) and total iron release (d) along the B-nZVI and Ni/Fe NPs corrosion in water.

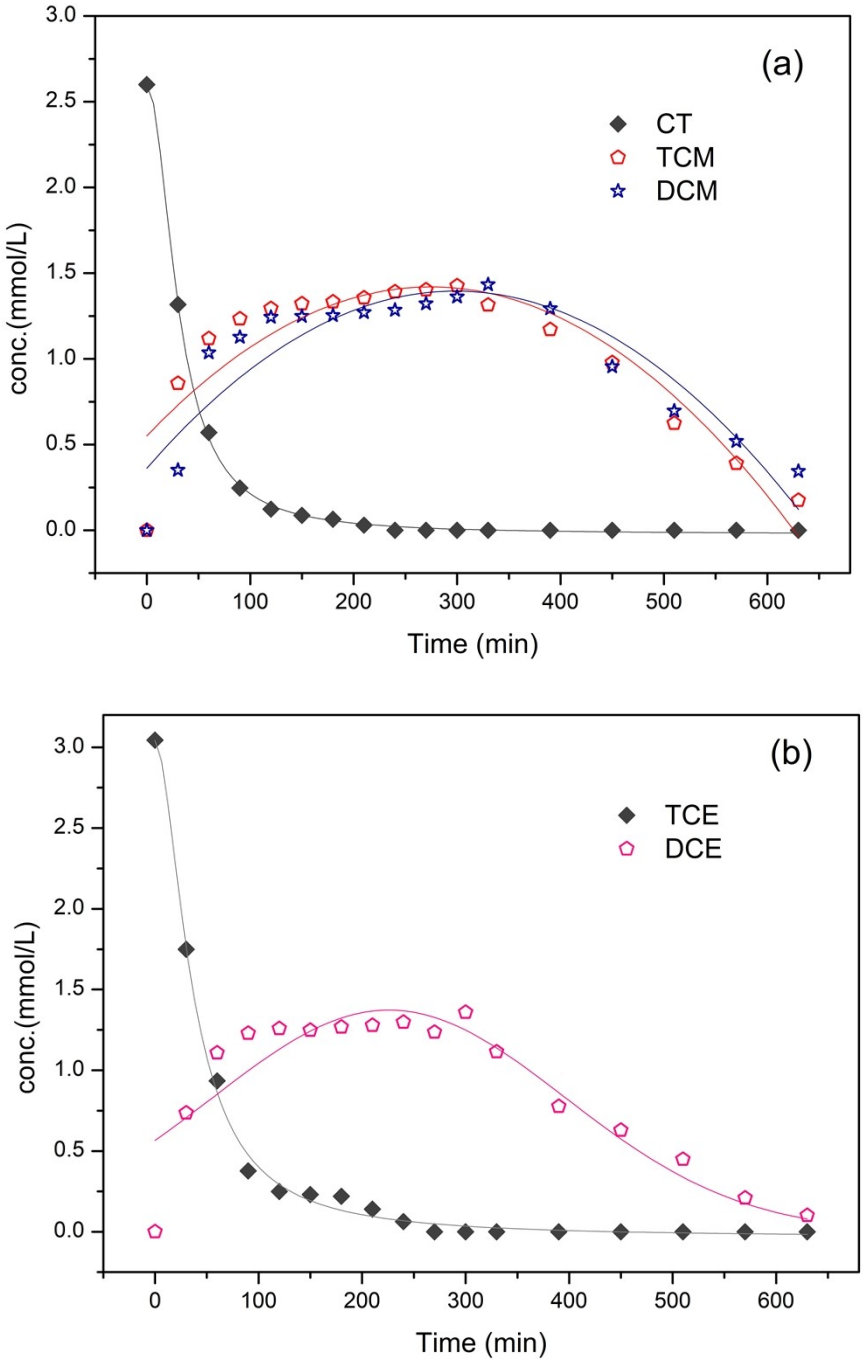

Figure s8. Long-term reductions of CT(a) and TCE(b) and corresponding by-products variation in 5wt% Ni/Fe system.

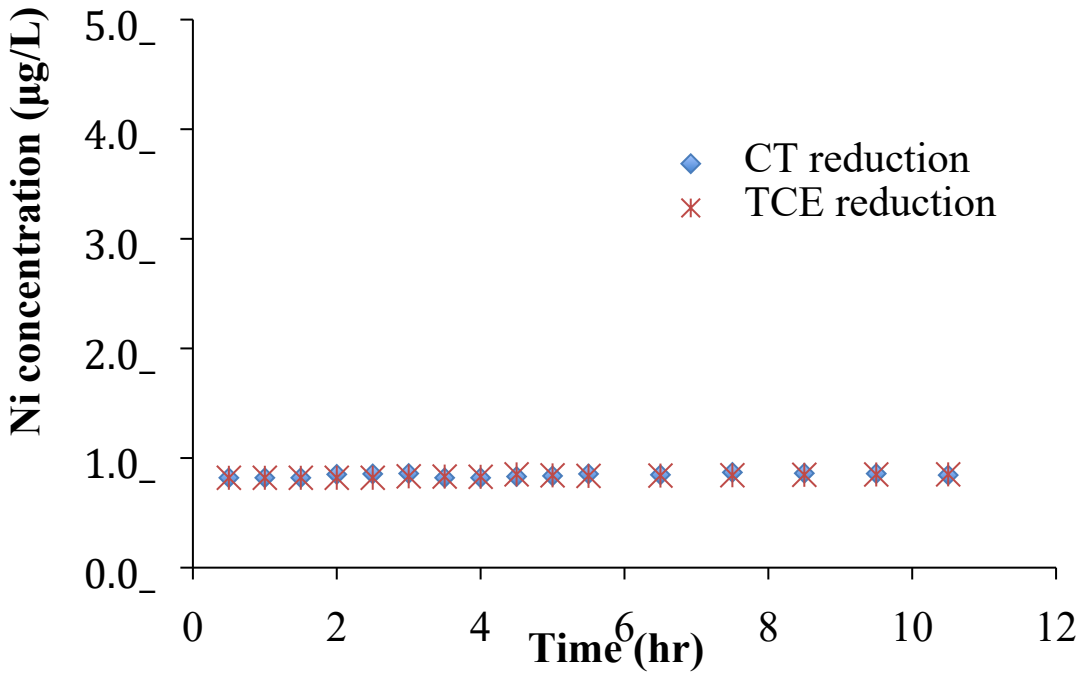

Figure s9. Ni release along the long-term reduction of CT and TCE.

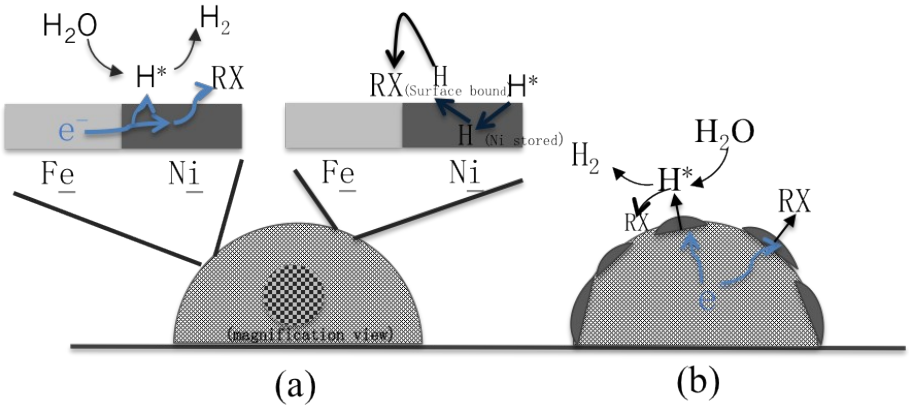

Figure s10 Conceptual model of the structures and reduction mechanisms of Ni/Fe NPs with low/medium nickel loading and high nickel loading.